JOURNAL OF Materials CHEMISTRY

Na–Li exchange of $Na_{1+x}Ti_{2-x}Al_x(PO_4)_3$ ($0.6 \leqslant x \leqslant 0.9$) NASICON series: a Rietveld and impedance study†

F. E. Mouahid,[a] M. Zahir,[a] P. Maldonado-Manso,[b] S. Bruque,*[b] E. R. Losilla,[b] M. A. G. Aranda,[b] A. Rivera,[c] C. Leon[c] and J. Santamaria[c]

[a]*L.P.C.M. Département de Chimie, Faculté des Sciences, Université Chouaib Doukkali, El Jadida, 24000, Morocco*
[b]*Departamento de Química Inorgánica, Cristalografía y Mineralogía, Universidad de Málaga, 29071 Málaga, Spain. E-mail: bruque@uma.es*
[c]*Departamento de Física Aplicada III, Universidad Complutense de Madrid, 28040 Madrid, Spain*

Received 1st March 2001, Accepted 24th August 2001
First published as an Advance Article on the web 17th October 2001

Ion exchange reactions have been tested in sodium-containing NASICON materials in order to prepare $Li_{1+x}Al_xTi_{2-x}(PO_4)_3$ compounds with high lithium content, $x \geqslant 0.6$. However, the studied lithium exchange reactions are not complete and the final solids have an appreciable sodium content. Structural characterisation by the Rietveld method reveals that sodium partially remains at the M1 site and the M2 site is fully exchanged by Li^+ cations. The electrical properties have been characterised by an impedance study. The Li-exchanged NASICONs have lower dc conductivities and higher activation energies than the pure sodium analogues. This is likely due to the mixed alkali effect and because some percolation pathways are disabled.

Introduction

The discovery of NASICON (**Na** Super**I**onic **CON**ductor) materials[1,2] was an important finding in the solid electrolytes field as they provide a three-dimensional network that encloses channels where superionic conductivity may occur. The original NASICONSs were solid solutions derived from $NaZr_2P_3O_{12}$ by partial replacement of P by Si with Na excess to balance the negatively charged framework to yield the general formula $Na_{1+x}Zr_2P_{3-x}Si_xO_{12}$ ($0 \leqslant x \leqslant 3$). Since then, a large number of related materials has been synthesised, mainly phosphates. Related series are obtained by partial substitution of tetravalent M^{IV} cations by trivalent M^{III} ones to yield $Na_{1+x}M^{IV}_{2-x}M^{III}_x(PO_4)_3$.

In the 3D skeleton, described by the formula $[M^{IV}_{2-x}M^{III}_x(PO_4)_3]^{(1+x)-}$, PO_4 tetrahedra are linked by the corners to MO_6 octahedra. The infinite ribbons resulting from this linkage are connected together, perpendicular to the *c* direction, by PO_4 tetrahedra to form the framework. The Na^+ ions occupy two positions in the conduction channels: the M1 site (one per formula) is coordinated by a trigonal antiprism of oxygens, and the M2 site (three per formula) has a distorted 8-fold coordination. M1 and M2 sites are located inside and between the ribbons, respectively. An initial approach to correlate electrical parameters (ionic conductivities and activation energies) with generic average structural parameters (unit cell constants) was followed by scrutiny of specific structural factors such as the size of the bottleneck that connects the M1 and M2 sites.[3–5] However, to establish possible correlations of this type, full crystal structure information is required. This may be obtained either by single crystal diffraction or by Rietveld analysis of powder diffraction data.

On the other hand, Li cells have a very important market due to their unmatchable properties of high potential ($E^\circ = -3.024$ V), their very lightweight nature and, hence, very high energy-density storage properties. There is an intense research effort in the area of three-dimensional Li-based solid electrolytes for all solid lithium batteries. NASICON type materials with Li cations in the channels are candidates as electrolytes in these cells if the conductivity properties at room temperature are enhanced. $LiM_2(PO_4)_3$ (M = Ge, Ti, Sn, Zr, Hf) are known with the M = Ti system probably the most studied.[6] The small size of the Ti^{4+} cations makes the size of the sites in the channels more appropriate for lithium cations.

The ionic conductivity of $LiTi_2(PO_4)_3$ ($\sim 10^{-6}$ S cm^{-1} at RT) may be increased, by at least two orders of magnitude, upon partial substitution of Ti^{4+} by trivalent cations such as Al, Ga, In, Ti, Sc, Y, La, Cr or Fe.[7–17] The increase of ionic conductivity is due to a higher charge carrier number but is also due to a lower porosity of the pellets. The conductivities for $Li_{1+x}Ti_{2-x}Al_x(PO_4)_3$ materials can be as high as 10^{-3} S cm^{-1} at RT.[16] The ionic radius of Al^{3+} is likely to lie within the tolerability limit of the NASICON framework. The maximum amount of Ti^{4+} that can be replaced for Al^{3+}, with the concomitant insertion of Li^+ to balance the charges, is 0.4 per formula unit.[10,17]

In this paper, we report the synthesis, crystal structures and ionic conductivities of lithium derivatives of the $LiTi_2(PO_4)_3$ family by partial substitution of Ti^{4+} by Al^{3+}. The starting materials[18] were $Na_{1+x}Ti_{2-x}Al_x(PO_4)_3$ and the Na^+ by Li^+ ion exchange reaction was carried out with molten $LiNO_3$ in an attempt to increase the maximum amount of lithium in the NASICON structures [up to $Na_{1.9}Ti_{1.1}Al_{0.9}(PO_4)_3$]. However, we show that the ion exchange reaction is not complete and that the presence of Na^+ cations in the structure strongly decreases the ionic conductivity.

Experimental

Synthesis

$Li_{1+x}Ti_{2-x}Al_x(PO_4)_3$ samples were prepared by reaction of $Na_{1+x}Ti_{2-x}Al_x(PO_4)_3$ (**Na$_{1+x}$**) with a large excess of molten $LiNO_3$. The synthesis of the **Na$_{1+x}$** series has been reported.[18] Mixtures of **Na$_{1+x}$** ($x = 0.6$, 0.8 and 0.9) + n $LiNO_3$ with $n \sim 40$ were heated for 2 h at 300 °C, then cooled, washed with water

†Electronic supplementary information (ESI) available: Selected bond angles for the $(Li,Na)_{1+x}Ti_{2-x}Al_x(PO_4)_3$ series. See http://www.rsc.org/suppdata/jm/b1/b102918p/

 DOI: 10.1039/b102918p

thoroughly and dried. Two successive treatments were carried out in order to shift the equilibrium toward the maximum exchange. The exchanged materials still contain some sodium and they are denoted as $\mathbf{LiNa_{1+x}}$.

Chemical analysis

Samples ($\sim$50 mg) were dissolved in a mixed aqueous solution of 40% w/w HF acid–60% w/w HNO_3 acid (5 : 2) at 50 °C and the lithium contents were determined by emission atomic spectroscopy in air/acetylene flame. K was added (K/Li ratio: 1000/1) to avoid lithium ionisation.

X-Ray diffraction. X-Ray powder diffraction patterns were collected on a Siemens D5000 automated diffractometer with ($\theta/2\theta$) Bragg–Brentano geometry using graphite monochromated Cu-K$\alpha_{1,2}$ radiation. The XRD patterns were recorded in the range 2θ 12–50° for indexing purposes and to follow the chemical reactions. Patterns were collected in the range 2θ 14–125° with 0.03° step size for 14 s (counting time) in order to refine the crystal structures by the Rietveld method.[19]

Thermal analysis

Thermogravimetric and differential thermal analyses (TG–DTA) were performed for all compositions on a Rigaku Thermoflex TG8110 apparatus. The temperature was varied from RT up to 900 °C at a heating rate of 10 K min^{-1} with calcined Al_2O_3 as reference.

Ionic conductivity

Complex admittance was measured using a Hewlett Packard 4284A LCR meter, in the frequency range 20 Hz–1 MHz, at various temperatures. The data acquisition was computer controlled, using the IEEE 488 standard. The samples were cylindrical pellets 10 mm in diameter and 1.5 mm thick, on whose faces silver colloidal paint was deposited. The pressure was 100 MPa and the sintering conditions of the pellets were 725 °C for 12 h. Higher temperatures led to the thermal decomposition of the samples giving mainly $AlPO_4$. Measurements were conducted under an N_2 flow to ensure an inert atmosphere. The pellet densities were determined from their masses and volumes. The relative densities of the pellets (compaction degree) were calculated taking into account the crystallographic densities.

Results and discussion

Ion exchange study

The NASICON materials exhibit cation exchange properties. This allows new phases to be obtained by high temperature ion exchange[20] with molten $LiNO_3$ or $AgNO_3$ or alternatively by refluxing with a dissolved lithium salt.[21] The ion exchange reaction described in the experimental section was planned to extend the maximum lithium content in this NASICON series. $Na_{1+x}Ti_{2-x}Al_x(PO_4)_3$ ($x<1.0$) can be easily prepared by direct solid state synthesis.[18] However, $Li_{1+x}Ti_{2-x}Al_x(PO_4)_3$ ($x>0.5$) can not be directly prepared.[10,17] Thus, ion exchange is attempted to prepare solids with composition $Li_{1+x}Ti_{2-x}Al_x(PO_4)_3$ ($0.5<x<0.9$). Our synthetic study has revealed that the second ion exchange reaction did not improve the exchange ratio. Hence, no further cycles were attempted. The lithium contents were determined from atomic emission spectroscopy and the alkali metal contents are given in Table 1. It should be noted that the lithium content due to an impurity phase, Li_3PO_4, quantified by the Rietveld method (see below), has been taken into account and the lithium contents given in Table 1 are those in the NASICON phases. The sodium contents, given in Table 1, are calculated to balance the charges. Unfortunately, the exchange ratios are of the order of 50% and sodium is still present to an appreciable degree in the NASICON samples as confirmed by the structural study by the Rietveld method. Thermal studies did not show any mass loss between room temperature and 800 °C. DTA data did not show any structural transition on heating but melting was observed above *ca.* 800 °C.

Ion exchange by refluxing was also tested following the procedure giving in ref. 21. $\mathbf{Na_{1+x}}$ pristine samples were refluxed with LiCl in *n*-hexanol (Na : Li molar ratio 1 : 20) for four days. However, the Na/Li exchanged ratios were lower than those obtained from molten $LiNO_3$. Hence, these samples were not characterised further.

Structural study

Initial XRD data indicated that the three $\mathbf{LiNa_{1+x}}$ samples were crystalline with structures belonging to the $R\bar{3}c$ NASICON-type. A small amount of lithium orthophosphate, Li_3PO_4, was also detected in the samples. The crystal structures were refined from XRD data by the Rietveld method with the GSAS suite of programs[22] using the $R\bar{3}c$ structures of $\mathbf{Na_{1+x}}$ pristine samples as starting models.

The nominal Ti/Al compositions were randomly distributed in the octahedral site. Full occupancy of the Li(1) site at (000) (6b Wyckoff notation) and excess lithium located in the Li(2) site at (0.6 0 ¼) (18e) was initially postulated. The common overall parameters, histogram scale factor, background coefficients, unit-cell parameters, zero-shift error and pseudo-Voigt coefficients were refined. Once the patterns were refined to low *R*-values, the remaining sodium atoms were located in the structure. To do so, two constrained refinements to force the electroneutrality with Na at the M1 and M2 sites, respectively, were carried out. Na at the M2 site converged to zero but the presence of sodium at the M1 site reduced the *R*-factors notably. Hence, the occupation factors of Li(2) site were also fixed to the nominal values and the fractions of Na and Li at M1 were refined constrained to full occupancy. Isotropic temperature factors for each site were refined but those of the M1 and M2 sites were fixed to reasonable values, $U_{iso}=0.025$ Å^2. The unit cell parameters and the *R*-agreement Rietveld factors are given in Table 1. The weight fractions of the side-phase, Li_3PO_4, are also given in Table 1. The refined positional and thermal atomic parameters are given in Table 2. Refined bond distances are given in Table 3 and the bond angles are given as ESI.† The Rietveld plot for the sample $(LiNa)_{1.6}Ti_{1.4}Al_{0.6}(PO_4)_3$ is shown in Fig. 1 as an example of the fit in this series.

The unit cell variations along the $\mathbf{LiNa_{1+x}}$ series are given in Fig. 2. The cell variations of the pristine materials, Na_{1+x} series,[18] and pure low lithium content $Li_{1+x}Ti_{2-x}Al_x(PO_4)_3$ series[23] are also shown in Fig. 2. The values of the cell parameters and their variation for $\mathbf{LiNa_{1+x}}$ confirm the Rietveld results. Lithium enters in the M2 sites which decreases the length of the *a*-axis. However, the *c*-axis is much more sensitive

Table 1 Analytical and structural data for $(Li,Na)_{1+x}Ti_{2-x}Al_x(PO_4)_3$ samples

x	Overall compositions	a/Å	c/Å	V/Å^3	R_{wp} (%)	R_F (%)	Li_3PO_4 (%w/w)
0.6	$Li_{0.77}Na_{0.83}$	8.4435(3)	21.636(1)	1335.8(1)	12.14	2.02	1.5(1)
0.8	$Li_{0.88}Na_{0.92}$	8.4203(4)	21.592(1)	1325.8(1)	12.25	1.95	5.5(3)
0.9	$Li_{1.25}Na_{0.65}$	8.4001(8)	21.550(2)	1316.9(3)	16.84	4.40	1.9(2)

Table 2 Refined structural parameters for the $(Li,Na)_{1+x}Ti_{2-x}Al_x(PO_4)_3$ series. The refined phase compositions are $Li_{0.72(2)}Na_{0.88}$, $Li_{1.09(2)}Na_{0.71}$ and $Li_{1.45(2)}Na_{0.45}$, for $x=0.6$, 0.8 and 0.9, respectively

		$Al_{0.6}$	$Al_{0.8}$	$Al_{0.9}$
Li(2) (18e) (x 0 ¼)	x	0.53(1)	0.55(1)	0.58(1)
	Fraction Li	0.20(—)	0.267(—)	0.30(—)
M(1) (6b) (0 0 0)	$U_{iso}\times100$	2.5(—)	2.5(—)	2.5(—)
	Fraction Li	0.12(2)	0.29(2)	0.55(2)
Ti–Al (12c)	z	0.1453(1)	0.1451(1)	0.1454(2)
(0 0 z)	$U_{iso}\times100$	0.0(1)	0.2(1)	0.8(2)
P (18e)	x	0.2861(3)	0.2860(4)	0.2838(7)
(x 0 ¼)	$U_{iso}\times100$	1.0(1)	1.3(1)	1.9(2)
O(1) (36f)	x	0.1720(6)	0.1713(6)	0.1675(11)
(x y z)	y	−0.0287(6)	−0.0311(7)	−0.0312(12)
	z	0.1918(2)	0.1924(3)	0.1922(5)
	$U_{iso}\times100$	1.5(2)	2.1(2)	3.7(4)
O(2) (36f)	x	0.1917(5)	0.1909(6)	0.1908(10)
(x y z)	y	0.1630(5)	0.1610(6)	0.1609(9)
	z	0.0878(2)	0.0887(3)	0.0891(5)
	$U_{iso}\times100$	0.3(1)	0.9(2)	1.9(3)

Table 3 Selected interatomic distances for $(Li,Na)_{1+x}Ti_{2-x}Al_x(PO_4)_3$ series

	$Al_{0.6}$	$Al_{0.8}$	$Al_{0.9}$
A–O(1) × 3	1.879(4)	1.890(5)	1.854(8)
A–O(2) × 3	1.957(4)	1.931(5)	1.924(9)
P–O(1) × 2	1.530(4)	1.514(5)	1.523(9)
P–O(2) × 2	1.526(4)	1.534(4)	1.542(7)
M(1)–O(2) × 6	2.429(5)	2.431(6)	2.432(10)
Li(2)–O(1) × 2	3.46(8)	3.32(6)	3.12(8)
Li(2)–O(1) × 2	2.56(1)	2.55(1)	2.54(1)
Li(2)–O(2) × 2	1.74(6)	1.84(5)	2.02(8)
Li(2)–O(2) × 2	2.54(4)	2.46(3)	2.36(3)
M(1)···Li(2) × 6	3.04(1)	3.05(1)	3.09(2)
Li(2)···Li(2) × 4	4.25(2)	4.27(2)	4.35(5)
Li(2)···Li(2) × 4	4.362(6)	4.363(7)	4.382(15)

to the M1 site composition, and the presence of sodium in this site causes the variation of the length of the c-axis upon ion exchange to be negligible. Fully exchanged samples with high Li content are expected to have lower values of the c-axis, of the order of 21.0 Å instead of 21.6 Å, see Fig. 2. The presence of Na in the M1 site is very important as it results in the 'mixed alkali' effect which is discussed below. Probably, Li prefers the M2 site because a location slightly out of the M2 cavity centre allows a coordination environment with short Li–O bond distances.[24,25] The situation in the M1 cavity is poorer as a displacement of Li from the M1 centre leads to only three short Li–O distances with the remaining bonds too long.

Impedance study

The experimental results indicate clear blocking phenomena at grain boundaries and electrode characteristics of ionic conductors. Fig. 3 shows complex impedance plots for a representative sample at two temperatures. At high temperatures, well developed spikes, characteristic of blocking electrodes, can be observed at low frequencies. Fig. 3 also shows the associated capacitance of the lowest frequency at 469 K for the $LiNa_{1.8}$ sample (0.1 μF). At lower temperatures, a depressed/deformed semicircle is observed. The deformation may be related to the presence of a second semicircle at lower frequencies due to the partial blocking (constriction effect) of the grain boundaries. To further examine this point Fig. 4 shows the real part of the complex capacitance (C') as a function of frequency for the same sample. A pronounced increase can be observed at low frequency which is associated with charge pile up at the blocking silver electrodes. The high temperature capacitance shows a small degree of saturation towards values in the 100 nF range. At higher frequencies a clear relaxation is observed from values of 10 pF to a high frequency value in the pF range. This relaxation, most likely, results from the constriction effect at grain boundaries, and can be modelled in terms of the series association of two parallel circuits: one corresponding to the grain boundary region and the other to

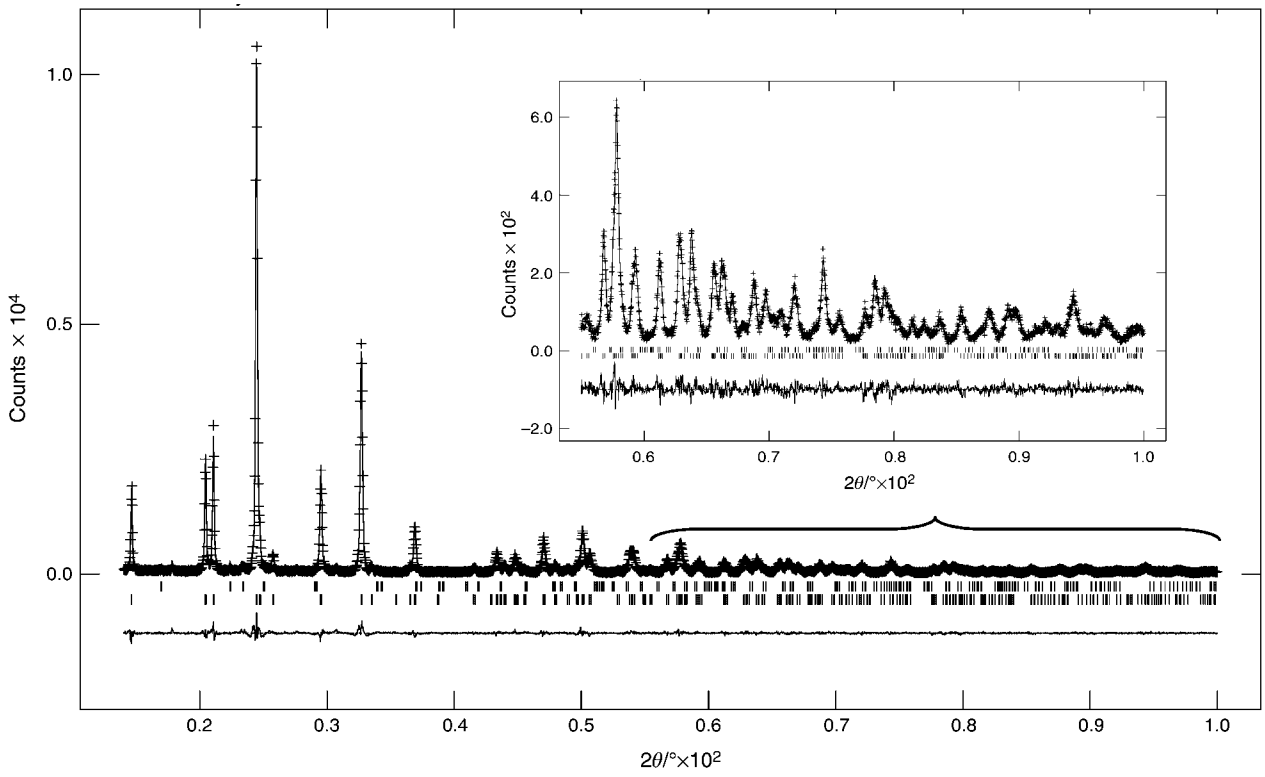

Fig. 1 Observed, calculated and difference laboratory X-ray diffraction patterns for $(Li,Na)_{1.6}Ti_{1.4}Al_{0.6}(PO_4)_3$.

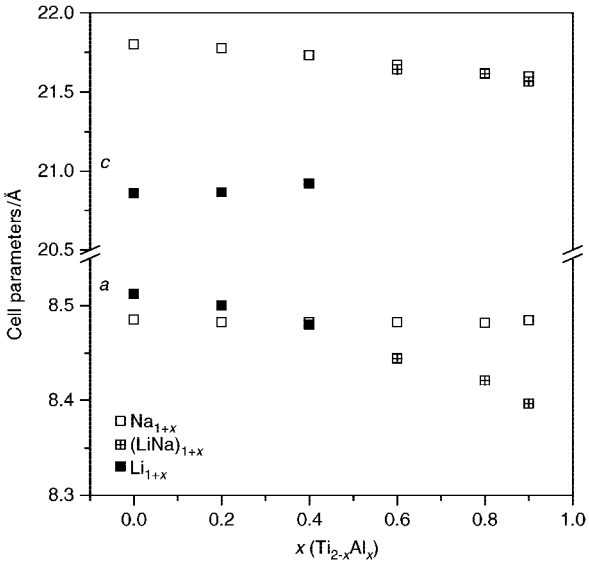

Fig. 2 Variation of lattice parameters for the $\mathbf{LiNa_{1+x}}$ series. Values for the $\mathbf{Na_{1+x}}$ and $\mathbf{Li_{1+x}}$ series are also given, see text.

the bulk response. The clear grain boundary contribution probably arises from the relatively low pellet density (see Table 4), however its capacitance contribution only exceeds the bulk value by one order of magnitude, and its resistance is also within the same order of magnitude as the bulk contribution. This indicates a relatively good connectivity between grains, which probably results from small amounts of Li_3PO_4 impurity phase acting as an intergrain binder.

Fig. 5 shows modulus data at different temperatures for the same composition on a double-logarithmic scale. Well defined maxima can be observed showing clear power law behaviour at both sides of the peak. Since the electric modulus scales with the inverse of the capacitance, the high capacitance contributions due to blocking or constriction effects are obscured in this representation, and the modulus peak can be used to describe the bulk contribution to the electrical conductivity relaxation.

A deeper insight into the electrical microstructure of the pellets can be obtained from the spectroscopic plots of the imaginary impedance contribution, Z'', and the complex electric modulus, M''. A selected plot for $\mathbf{LiNa_{1.8}}$ at 334 K is shown as the inset in Fig. 5. The maxima of both curves are

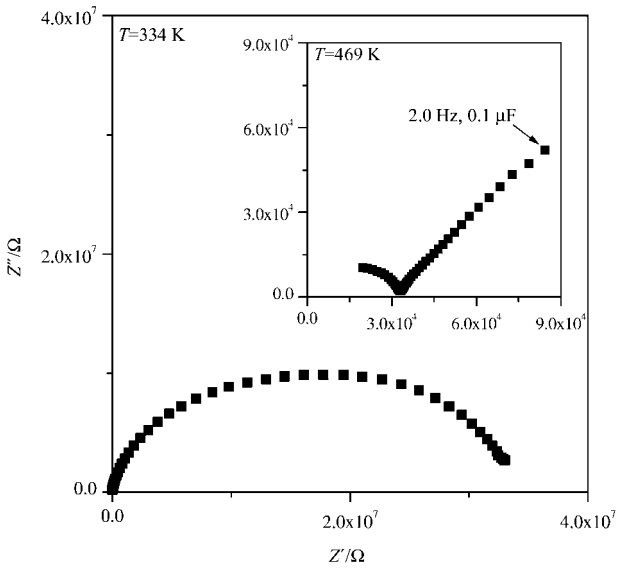

Fig. 3 Complex impedance plane plot for $\mathbf{LiNa_{1.8}}$ at 334 K (inset: 469 K).

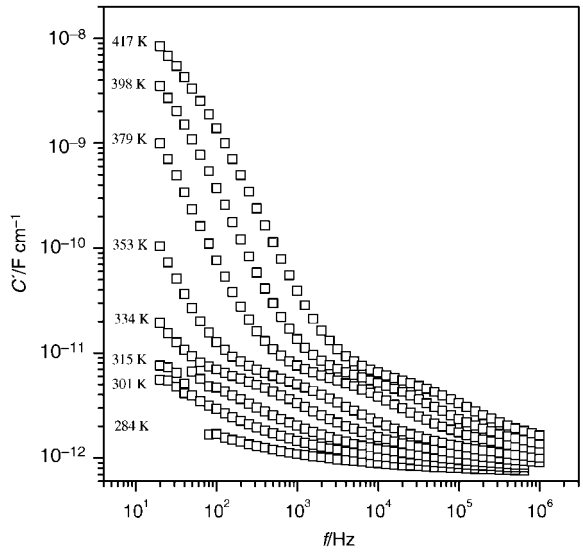

Fig. 4 Real part of the complex capacitance *vs.* frequency at several selected temperatures for $\mathbf{LiNa_{1.8}}$.

only separated by about one decade in frequency. This small separation again points to a relatively good grain connectivity.

Fig. 6 shows conductivity data in the frequency range 20 Hz–1 MHz at several temperatures for the same composition. The frequency dependence of the real part of the conductivity shows a low-frequency plateau and a crossover to a power-law dependence at high frequencies. This well-known behaviour, characteristic of ion hopping, can be described according to a complex conductivity $\sigma^*(\omega)$ of the form $\sigma^*(\omega)=\sigma_{dc}[1+(i\omega/\omega_p)^n]$ where σ_{dc} is the dc conductivity, ω_p is a crossover frequency, and the exponent n is related to the degree of correlation among moving ions. Values around 0.6 were typically obtained being quite similar for the three samples. Although no clear grain boundary contribution is observed in these plots, it is important to remark that conductivity values obtained from the low frequency conductivity plateaus can be influenced by the grain boundary contribution, and thus the bulk conductivity obtained from admittance curve fitting can be only taken as approximate.

Fig. 7 shows bulk conductivity plots, obtained from the above fitting, against the inverse of temperature for the $\mathbf{LiNa_{1+x}}$ series. Related data for the pristine series $\mathbf{Na_{1+x}}$ are given for comparison. Bulk conductivities at 400 K and the activation energies were obtained from the Arrhenius representations and are listed in Table 4. A straightforward method to check if these activation energies are truly associated to the bulk contribution is to use the frequency of the modulus peaks, f_{max}. As shown above, the modulus is not influenced by the grain boundary contribution, and since the peak frequency scales as the bulk conductivity over the bulk permittivity (σ/ε), provided the bulk capacitance is temperature independent, f_{max} is equally activated as the conductivity. The inset of Fig. 7 shows the Arrhenius representation of the $\log f_{max}$ for the three samples. Activation energies obtained from both Arrhenius plots (σ_{bulk} and $\log f_{max}$) agree within ± 0.02 eV. This supports that the conductivity values obtained from the conductivity fits are good estimates of the bulk contribution. Conductivities and activation energies do not change appreciably along this series. It is worthwhile to note that this method is usually quite

Table 4 Electrical data for $(Li,Na)_{1+x}Ti_{2-x}Al_x(PO_4)_3$ samples

x	$\sigma_{400\,K}$/S cm^{-1}	E_a/eV	Compaction degree (%)
0.6	9.4×10^{-7}	0.59(2)	72(3)
0.8	1.5×10^{-6}	0.66(1)	70(3)
0.9	7.9×10^{-7}	0.62(1)	65(3)

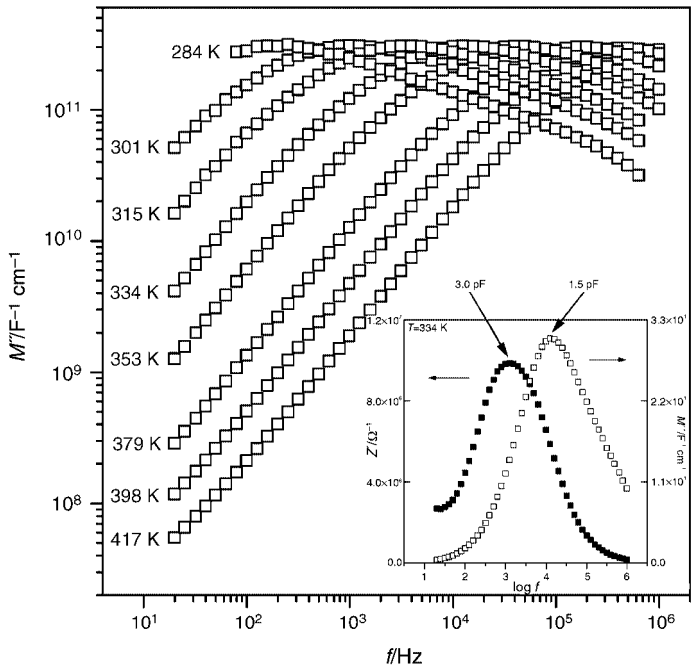

Fig. 5 Imaginary part of the modulus *vs.* frequency at several selected temperatures for $LiNa_{1.8}$. The inset shows the spectroscopic plots of Z'' and M'' *vs.* $\log f$ at 334 K.

reliable as it avoids the possible errors associated to the fittings and it is very fast and easy. However, it does not provide bulk conductivities for samples showing strong departures from ideal Debye responses.

General discussion

The $Li_{1+x}Al_xTi_{2-x}(PO_4)_3$ series with NASICON structure is one of the most appropriate systems to accommodate Li cations because of the small size of the AlO_6 octahedra. This has been highlighted by many authors, however, the direct synthesis of this series with $x \geqslant 0.4$ leads invariably to $AlPO_4$ as a side-phase with berlinite or trydimite structures.[8,11,17] On the other hand, we have shown that the direct synthesis of $Na_{1+x}Al_xTi_{2-x}(PO_4)_3$ is possible up to $x \leqslant 0.9$.[18] This NASICON series has a suitable negative charged framework, with the aluminium already incorporated in the network, to accommodate lithium in the M1 and M2 sites. The objective of this study was to extend the lithium content that can be prepared by direct synthesis. Furthermore, our idea was to carry out the ion exchange reactions at much lower temperatures than those of the direct synthesis, in order to prevent the formation of $AlPO_4$.

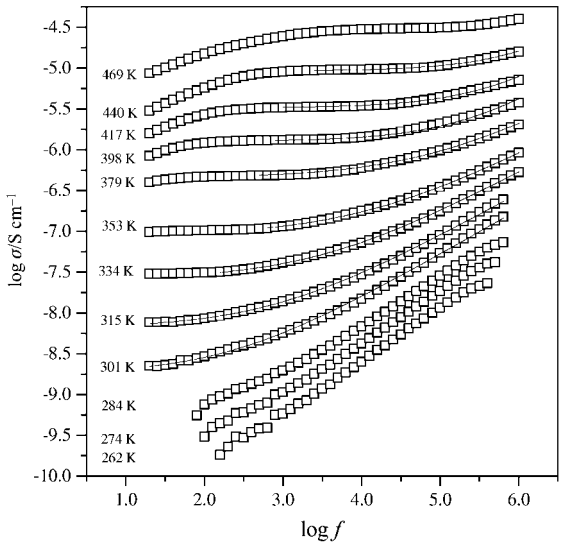

Fig. 6 Real part of the overall conductivity *vs.* frequency at several seleted temperatures for $\mathbf{LiNa_{1.8}}$.

However, the ion exchange reactions are not complete. The sodium at the M1 site is not fully exchanged since the Li/Na ratio in this site was quite low. If the only Li^+ diffusion pathway is M1–M2, then, it is difficult to rationalize the very high lithium ratio at the M2 site and the quite low Li ratio at the M1 site. However, it has been recently suggested[26] that the conduction pathway in NASICONS may be ···M1–M2–M1··· or ···M2–M2··· depending upon the composition of the series and their corresponding crystal structures. If Li can move across the M2 sites, then these sites may be fully exchanged whereas sodium, which is quite well coordinated in the M1 site, is not so exchanged.

Several factors can contribute to the lower conductivities and slightly higher activation energies of the studied $\mathbf{LiNa_{1+x}}$ series when compared to the pure-sodium pristine materials, $\mathbf{Na_{1+x}}$. It is of note that $Na_{1.9}$ has a bulk conductivity two orders of magnitude higher than $LiNa_{1.9}$, see Fig. 6, despite having the same vacancy content.

Since the occupancy of sodium at the M1 sites is high this makes the conductivity due to the lithium cations highly difficult across M1–M2 bottlenecks; Na^+ may block lithium diffusion along the M1–M2 pathway. This may be related to the mixed alkali effect studied mainly in glasses. It has been repeatedly reported that a pronounced reduction in conductivity is observed in oxide glasses with two or more different types of alkali components when compared to the analogous single-alkali glasses.[27,28] It is noteworthy that in the present samples, the M1 oxygen environment is appropriate for Na^+ cations but is too large for Li^+ cations, see Table 3.

Lithium at the M2 site should be situated off-centre in the M2 cavity close to the bottleneck to optimise the oxygen bond distances. They are also likely displaced to minimise the $Na^+(1)$–$Li^+(2)$ interactions. The low scattering factor of Li^+ cations rules out their precise location. The observed cation configuration is more shielded with lower repulsion between monovalent charge carriers which makes the ion hopping energetically unfavoured.

Lithium ions may diffuse across the M2–M2 bottlenecks but

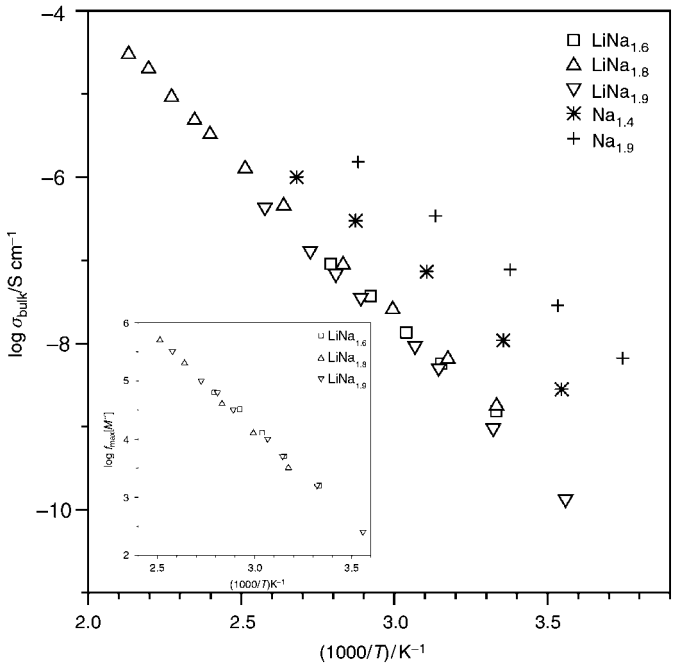

Fig. 7 Variation of log σ_{bulk} *vs.* 1000/*T* for $\mathbf{LiNa_{1+x}}$ series. Two selected samples of $\mathbf{Na_{1+x}}$ series are also given for comparison. The inset shows the Arrhenius variation of log f_{max} from the complex modulus.

the values of conductivity and activation energy can not be directly compared to those of the pristine materials where M1–M2 hopping is favoured.

On the other hand, if Na^+ is the main charge carrier, then, lithium will partially block their mobility. A Li and Na NMR study is in progress to elucidate the nature of the charge carrier in these solids.

Conclusion

$Na_{1+x}Al_xTi_{2-x}(PO_4)_3$ has been lithium exchanged using molten $LiNO_3$ to prepare $Li_{1+x}Al_xTi_{2-x}(PO_4)_3$ materials with high lithium content. Unfortunately, the ion exchange reactions are not complete and the final solids have variable sodium contents at the M1 site. The crystal structures of these solids have been characterised by Rietveld studies and the electrical properties have been characterised by an impedance study. The $LiNa_{1+x}$ NASICONs have lower dc conductivities and higher activation energies than the pure sodium analogues. This may result from ion pathway blocking as a result of different mobilities of the two conducting species and might be an indication of a mixed alkali effect in inorganic materials, which, to the best of our knowledge, has never been observed. Further work will be devoted in the future to clarify this issue.

Acknowledgements

We are grateful for the financial support from Programa Andaluz de Cooperación Internacional al Desarrollo from Junta de Andalucía. This work was also partly supported by the MAT2000-1585-C3-3 research grant of CICYT.

References

1 H. Y-P. Hong, *Mater. Res. Bull.*, 1976, **11**, 173.
2 J. B. Goodenough, H. Y-P. Hong and J. A. Kafalas, *Mater. Res. Bull.*, 1976, **11**, 203.
3 H. Kholer and H. Schulz, *Mater. Res. Bull.*, 1986, **21**, 23; H. Kholer and H. Schulz, *Mater. Res. Bull.*, 1985, **20**, 1461; H. Kholer and H. Schulz, *Solid State Ionics*, 1983, **9–10**, 795.
4 E. R. Losilla, M. A. G. Aranda, S. Bruque, M. A. Paris, J. Sanz and A. R. West, *Chem. Mater.*, 1998, **10**, 665.
5 E. R. Losilla, M. A. G. Aranda, S. Bruque, M. A. Paris, J. Sanz, J. Campo and A. R. West, *Chem. Mater.*, 2000, **12**, 2134.
6 M. A. Paris and J. Sanz, *Phys. Rev. B*, 1997, **55**, 14270, and references therein.
7 M. A. Subramanian, R. Subramanian and A. Clearfield, *Solid State Ionics*, 1986, **18-19**, 562.
8 S. C. Li, J-Y. Cai and Z-X. Lin, *Solid State Ionics*, 1988, **28–30**, 1265.
9 H. Aono, E. Sugimoto, Y. Sadaoka, N. Imanaka and G. Adachi, *J. Electrochem. Soc.*, 1989, **136**, 590.
10 H. Aono, E. Sugimoto, Y. Sadaoka, N. Imanaka and G. Adachi, *J. Electrochem. Soc.*, 1990, **137**, 1023.
11 H. Aono, E. Sugimoto, Y. Sadaoka, N. Imanaka and G. Adachi, *Chem. Lett.*, 1990, 1825.
12 H. Aono, E. Sugimoto, Y. Sadaoka, N. Imanaka and G. Adachi, *Solid State Ionics*, 1990, **40–41**, 38.
13 H. Aono, E. Sugimoto, Y. Sadaoka, N. Imanaka and G. Adachi, *Bull. Chem. Soc. Jpn.*, 1992, **65**, 2200.
14 K. Ado, Y. Saito, T. Asai, H. Kageyama and O. Nakamura, *Solid State Ionics*, 1992, **53–56**, 723.
15 H. Aono, E. Sugimoto, Y. Sadaoka, N. Imanaka and G. Adachi, *Solid State Ionics*, 1993, **62**, 309.
16 J. Fu, *Solid State Ionics*, 1997, **96**, 195.
17 S. Wong, P. J. Newman, A. S. Best, K. M. Nairn, D. R. MacFarlane and M. Forsyth, *J. Mater. Chem.*, 1998, **8**, 2199.
18 F. E. Mouahid, M. Bettach, M. Zahir, P. Maldonado-Manso, S. Bruque, E. R. Losilla and M. A. G. Aranda, *J. Mater. Chem.*, 2000, **10**, 2748.
19 H. M. Rietveld, *J. Appl. Crystallogr.*, 1969, **2**, 65.
20 F. d'Yvoire, M. Pintard-Screpel, E. Bretey and M. Rochere, *Solid State Ionics*, 1983, **9–10**, 851.
21 K. Yoshida, K. Toda, K. Uematsu and M. Sato, *Key Eng. Mater.*, 1999, **157–158**, 289.
22 A. C. Larson and R. B. von Dreele, GSAS program, Los Alamos National Lab. Rep. No. LA-UR-86-748, 1994.
23 A. Boireau, LL. Soubeyroux, R. Olazcuaga, C. Delmas and G. L. Flem, *Solid State Ionics*, 1993, **63–65**, 484.
24 P. R. Slater and C. Greaves, *J. Mater. Chem.*, 1994, **4**, 1463.
25 M. Cretin and P. Fabry, *J. Eur. Ceram. Soc.*, 1999, **19**, 2931.
26 D. Mazza, *J. Solid State Chem.*, 2001, **156**, 154.
27 A. Bunde and P. Maass, *Physica A*, 1993, **200**, 80.
28 M. Tomozawa, *J. Non-Cryst. Solids*, 1993, **152**, 59.